A. HARA*[#], H. KAZIMIERCZAK*, A. BIGOS*, Z. ŚWIĄTEK*, P. OZGA*

EFFECT OF DIFFERENT ORGANIC ADDITIVES ON SURFACE MORPHOLOGY AND MICROSTRUCTURE OF Zn-Mo COATINGS ELECTRODEPOSITED FROM CITRATE BATHS

The effect of cationic, anionic and nonionic surface active additives, organic compounds and polymers on the electrodeposition of Zn-Mo coatings on steel substrate and detailed characterization in chosen optimal conditions was studied. The influence of polyethylene glycol (PEG) various concentration, sodium dodecyl sulphate (SDS), triton X-100, d-sorbitol, cetyl trimethyl ammonium bromide (CTAB), thiourea and disodium ethylenediaminetetraacetate (EDTA) on the electrodeposition process was examined. The composition of deposits was defined by wavelength dispersive X-ray fluorescence spectrometry (WDXRF). Results has shown that the current efficiency of the electrodeposition of Zn-Mo coatings is 71.4%, 70.7%, 66.7% for 1.5 g/dm^3 PEG 20000, 0.1 g/dm^3 Triton X-100 and 0.75 M D-sorbitol respectively.

The surface topography and roughness of selected coatings on steel was investigated by atomic force microscopy (AFM). The attendance of D-sorbitol of 0.75 M in the solution cause clear reduction of grain size and the value of roughness parameter (Ra) in relation to SDS, PEG, Triton X-100 and the sample prepared without the additives. The morphology of electrodeposited layers was studied by scanning electron microscopy (SEM). The addition of selected additives to the electrolytic bath results in the formation of smoother, brighter and more compact Zn-Mo coatings in comparison to layers obtained from similar electrolytes but without the addition of surfactants. The optimal concentration of the most effective additives such as PEG 20000, Triton X-100 and D-sorbitol is 1.5 g/dm^3, 0.1 g/dm^3, 0.75 M respectively.

Keywords: zinc-molybdenum alloy, citrate bath, electrodeposition, organic additives

1. Introduction

Corrosion-resistant coatings based on zinc have been widely used to protect steel. What is important, Zn serves as a sacrificial anode when is used as a coating on steel, which means that the substrate is protected even when the film has a discontinuities. To provide a longer term of anti-corrosion protection, zinc is generally covered with conversion layer of chromium (VI) compound which is highly toxic and carcinogenic and according to legal regulations should be eliminated. Zn-Mo alloy layers are environmentally friendly replacement materials. Furthermore it is known that the addition of molybdenum improves corrosion resistance, abrasion, hardness and toughness. Mo can be electrodeposited in pure state from an aqueous solution only in the presence of another metal, which causes Mo codeposition. To date, it was stated that only ferrous metals induce molybdenum deposition, forming an alloy [1]. However, recent examination prove that Zn-Mo alloy can be electrodeposited from citrate solutions [2]. While the addition of a proper surfactant influences the physical and mechanical properties of electrodeposits.

The role of additives in the electrodeposition process is not yet clearly understood. It can be assumed that the use of surface active additives in electrolytic bath have an important influence on the growth and morphology of the layers obtained. These additives are commonly used to reduce or even suppress the instability phenomena within the boundary layer. Hence, strongly adsorbing organic agents can be able to create monolayers that redistribute the reactivity of the substrate and therefore lead to the production of smooth and thin metal overlayers. Moreover, the deposit structure can be further modified by current density, pH, concentration of metal ions, surfactants etc. [3-6]. Additives are usually organic compounds, which can be categorized in the following major categories, I – grain refiners, II – dendrite and roughness inhibitors, III – levelling agents, IV – wetting agents or surfactants [7]. The use of additives in aqueous electrolytic baths can cause promoting levelling, brightening the deposit, reducing grain size, internal stress, pitting, changing chemical composition and corrosion behavior. The adsorption of the levelling agents takes place preferentially on the protrusions of the growing layer, which cause the movement of the metal ions toward the hollows of the microprofile and their deposition there.

In recent years, many researchers have focused on the study of the influence of various additives to plating baths on the process of electrodeposition of coatings [4-32]. The role of examined in this work organic additives in electrodeposition

*   INSTITUTE OF METALLURGY AND MATERIAL SCIENCE, POLISH ACADEMY OF SCIENCES, 25 REYMONTA STR., 30-059 KRAKOW, POLAND

Correspondence address: a.hara@imim.pl

208

of zinc and zinc alloys as also their properties are presented in summary Table 1.

It has been shown that the addition of polymer such as polyethylene glycol (PEG) to electrolytic bath result in an improve of current efficiency in compare to baths without PEG. It indicate that PEG can suppress the hydrogen evolution reaction and consequently the deposition process exceeds the hydrogen evolution. The presence of PEG in electrolytic bath helps to achieve smooth and compact Zn-Mo layers and, what is important, PEG is not built in to the layer [7]. PEG molecule can suppresses dendritic growth by adsorption of several molecules of additive on the deposit surface and thus potential shifts to more negative value [9]. Guo et al. found that the presence of PEG and dodecyl sulfate sodium salt (SDS) in electrolytic bath makes that polymer can adsorb on the surface of the micelles of SDS. PEG with shorter chain clings easier to SDS micelles than PEG with longer chain [25].

Gomes et al. [15] indicated that anionic surfactant SDS can adsorb on the growing zinc deposit and block the electrocrystallization process. This inhibition depends on the size of the organic molecules and on the specific interactions between the surfactant and the substrate as well as on the surfactant and the deposit interaction. For the Zn deposits obtained from solution containing SDS the most intensive diffraction lines were (101) [15] and (102) [10], which correspond to crystallographic texture with high angle pyramids planes as the main texture component (i.e. planes (10.1) and (10.2) are parallel to substrate surface and directions of crystal growth are <10.1>||ND and <10.2>||ND), where ND is perpendicular direction to substrate surface). The crystallographic orientation changes because the metal's surface energy is modified by the adsorption of the organic molecules [15]. The presence of SDS in electrolytic bath makes the arrangement of Zn as hexagonal platelets layer by layer, parallel to each other and to the substrate, hence the basal plane (002) is the main texture component in these layers [10].

Sharma et al. noted that [9] the addition of nonionic surfactant Triton X-100 to electrolytic bath result in the improvement of current efficiency when compared to electrodeposition without the presence of Triton X-100. During the electrodeposition process from bath containing Triton X-100 both adsorption and complex formation phenomena may occur. The electrocrystallization process can be hampered by the adsorption of Triton X-100 molecules on the growing zinc deposit. The deposits obtained in the presence of Triton X-100 are more irregular, with a distinct morphology, constituted by cauliflower type agglomerates. Even though the crystallite size of obtained films decreases when the Triton X-100 concentration in electrolyte growth. Moreover, the addition of Triton X-100 may lead to the formation of ZnO. It may be due to the blocking effect of surfactants molecules adsorbed on the metal surface, which cause shift of deposition potential toward more negative values, and then result in the incomplete reduction of ZnO [15].

Pereira et al. [6] showed that when the concentration of D-sorbitol (organic compound) is higher than 0.05 M the adsorption of D-sorbitol molecules on the zinc substrate is possible which then inhibit the deposition process. This phenomenon is observed by the decrease of the cathodic current density and the shift of the potential to more negative values with increasing D-sorbitol concentration. It was also suggest, on the basis of SEM micrographs, that the sorbitate anions cause refinement of zinc crystallites as the sorbitol concentration in the plating baths increases.

Praveen Kumar et al. studied the effect of surfactant cetyl trimethyl ammonium bromide (CTAB) on the co-deposition of B_4C nanoparticles in Zn matrix and reported that it enhanced the nucleation rate and retardation in crystal growth leading to the smaller crystallite size of the deposit [10]. The influence of CTAB on the drop of the crystallite size of the deposit is also confirmed by Gomes et al. [15], Mehta et al. [26] and Maharana et al. [27]. CTAB is a cationic surfactant that have the positive charge, and hence it attracts the negative charged particles. As suggested, CTAB possess more covering power than SDS, and hence formerly influences the deposition process. The addition of CTAB to the plating bath promotes the formation of needle shaped grains of Zn. The earlier investigations have revealed the similar type of deposit with porous nature in the presence of CTAB [15]. It is noteworthy to mention that the porous nature of the coating is due to the needle shape grains. An adsorption of a cationic surfactant hinders the growth of crystallite and nucleation of the new crystallite takes place. However, the growth of the latter would also be stopped by the adsorption of the surfactant, hence the process results in a fine-grained structure. Furthermore, the morphology change can be related to a strong blocking effect of the cationic surfactant, which causes an enlargement of the nuclei renewal rates, leading to an increase of nuclei number and needle growth.
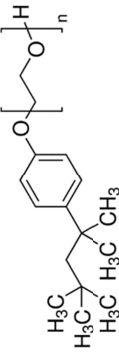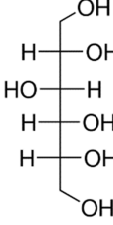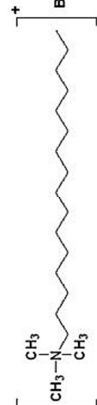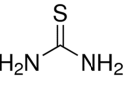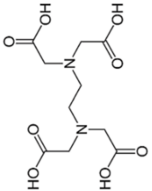
Sharma et al. [9] investigated the addition of organic compound thiourea on morphological and structural characteristics of obtained coatings. They showed that the thiourea is likely to suppress the hydrogen evolution reaction and improve the adsorption of PEG molecules on the metal surface. This type of synergetic effect is often observed when several additives are added to the electroplating baths resulting in a better surface finish and a refined grain size [9].

As a result, the current efficiency increase with the addition of thiourea. Moreover, the addition of thiourea may inhibit dendritic growth by adsorption of several molecules of additive on the deposit surface [9]. Such additive molecules adsorb readily on the cathode, thus regulating the reduction of zinc ions by either of two possible mechanisms: physical barrier or temporary metal complex formation. Moreover, it leads to the formation of a three-dimensional network of deposited zinc instead of a continuous plate film [14].

The influence of organic compound such as, disodium ethylenediaminetetraacetate (EDTA) on zinc electrodeposition process and on the morphology, structure and chemical composition of the electrodeposits was studied by Carvalho et al. [12]. They reported that zinc form complexes with EDTA. Zn^{2+} ions can form hydroxylated species, which are soluble or insoluble, depending on the pH solution. Therefore, in order

TABLE 1

The role of organic additives examined

structural formula	(structure)	(structure)	(structure)	(structure)	(structure)	(structure)	(structure)
additive	**SDS**	**PEG**	**Triton X-100**	**D-sorbitol**	**CTAB**	**Thiourea (Tu)**	**EDTA**
surfactant type	anionic	nonionic	nonionic	nonionic (pH<13)	cationic	nonionic (pH>0)	anionic
critical micelle concentrations (CMC)	8.2 mM	1 mM (PEG 300)	0.2-0.9 mM	—	1 mM	—	—
concentration range in bath used	0.05 g/dm³	0.25-1.5 g/dm³	0.1-1.5 ml/dm³	0.1-2 mol/dm³	0.05-1.0 g/dm³	0.1-1.5 g/dm³	0.05-0.2 mol/dm³
adsorption on zinc surface	Yes [15]		Yes [15]	Yes [6]	Yes [14-15,20,26]	Yes [14]	
suppress the hydrogen evolution reaction (improve of current efficiency)	Yes [15]	Yes [9]	Yes [9]		Yes [15]	Yes [9]	No [this paper]
suppress the dendritic growth		Yes [9]	Yes [9]		Yes [15,20,26]	Yes [14] No [this paper]	No – up to value 0,05 mol/l Yes – above 0,1 mol/l [this paper]
increase of zinc reduction overpotential		Yes [9]					
built in to the layer		No [7]					
complexing of zinc(II)			Yes [15]	Above pH 13		Yes [14]	Strong [12]
presence of ZnO in deposit layer			Yes [15]		Yes [15]		
reducing grain size	No [this paper]	Yes, strong [7]	Yes [9]	Yes [6]	Yes [14,15,20,26]	Yes [9]	Yes, faintly [12]
promoting levelling		Yes (2)			Yes (3) (4) (5) (6)		
synergy		Adsorption PEG onto SDS micelles (preferential PEG with shorter chain) [25]				Thiourea with PEG and Triton X-100 results in decrease of Zn grain size [9]	
preferential orientation	(101) [15] (102) [20] (high angle pyramids)		(101) [15] (high angle pyramids)		(100) [20] (110) [15] (prisms planes)		(002) [12] (basal plane)
molecule size (length, max. dimension)	~ 1.45 nm (~ 3.7 nm micelles, at 20 mM SDS) [24]	~ 26 nm (PEG 3000) ~ 170 nm (PEG 20000) (~ 0.38 nm/mer) [33]	~ 10.5 nm [34]	~ 0.74 nm	~ 1.96 nm	~ 0.25 nm	~ 0.88 nm

210

to avoid precipitation of Zn hydroxides, EDTA was proposed to complex the Zn^{2+} ions. XDR patterns indicated that the electrodeposits produced either from electrolytes with EDTA and without it, compose of pure Zn. These electrodeposited Zn coatings include crystallites preferentially oriented parallel to the (0 0 2) plane [12].

The purpose of this work was to optimize the electrodeposition of good quality, smooth and compact Zn-Mo coatings on steel using various kinds of additives to the plating baths and to detail characterization of obtain layers in chosen optimal conditions ensured by well-worked additives. In this research, the addition of polymer, organic compounds and various types of surfactants i.e. cationic, anionic and nonionic were studied. The work was divided into 2 stages. The first part base on the examination of seven additives and the selection of only optimally working. In the second part a detailed analysis of the coatings deposited with the addition of selected additives was performed.

2. Experimental

The solutions were prepared using deionized water (resistivity 18.2 MΩ·cm at 25°C) and analytical-grade reagents. The appropriate amount of sodium citrate up to 0.25 mol/dm^3, zinc sulphate up to 0.24 mol/dm^3, sodium molybdate 0.015 mol/dm^3 was dissolved in the water, and then organic compounds in various configuration were added: polyethylene glycol (PEG) up to 1.50 g/dm^3, sodium dodecyl sulphate (SDS) 0.05 g/dm^3, Triton X-100 up to 1.5 g/dm^3, D-sorbitol up to 2 M, CTAB up to 1 g/dm^3, Thiourea up to 1.50 g/dm^3, EDTA up to 0.20 M. The pH of plating baths was adjusted by the addition of sulphuric acid or sodium hydroxide.

The electrodeposition process was carried out in a conventional three-electrode system in a 50 cm^3 cell. A rotating disc electrode (RDE) was employed in all electrochemical experiments to provide constant and controlled hydrodynamic conditions. As the counter electrode a platinum sheet (12 cm^2) was used. A low-carbon steel disc (surface area 2.83 cm^2) was used as a working electrode. Steel electrodes were chemically polished in a proper mixture (2 cm^3 30% H_2O_2 with 14 ml oxalic acid 100 g/dm^3 and 40 cm^3 H_2O) in 40 °C. The electrochemical measurements were carried out galvanostatically, by means of potentiostat-galvanostat PGSTAT302N. The current density applied was –1.4 A/dm^2. The current efficiency was determined from the chemical analysis of deposits electroplated under selected conditions and the mass of deposits, using Faraday's law.

The composition of deposits was defined by wavelength dispersive X-ray fluorescence spectrometry (WDXRF). The WDXRF analysis was performed via a Rigaku Primini spectrofluorimeter using scintillation counters (LiF1 crystal).

The morphology of the obtained coatings was investigated by scanning electron microscopy (SEM) using an FEI E-SEM XL30.

Innova (Bruker) in tapping mode with the resolution of 512×512 points and the scan length of 20 μm was used for AFM analysis. The NCHV (Si doped with Sb) cantilevers with a spring constant of 42 N/m and a resonance frequency of 330 kHz were employed in AFM analysis.

The micro-Raman spectra were obtained at room temperature using a Renishaw inVia Raman microscope (backscattering geometry, Peltier cooled CCD camera, Leica microscope, 1800 lines mm^{-1} grating) with HeNe laser excitation of 633 nm and power 21 mW. The lateral and depth penetration resolution were about 1.0 μm and 1.8 μm respectively (Leica objective 100×).

The X-ray diffractometry (Philips diffractometer type X'Pert in the Bragg-Brentano geometry in a system with rotating sample) was used for determination of phases in the layer as also for determination of selected microstructure parameters i.e. crystallite sizes (D_{Cr}) and deformations of the crystal lattice in the crystallite (ε). To describe the profile of the diffraction line the function of pseudo-Voigt was used. The analysis of the profile of the diffraction line is a simple and effective method to estimate the crystallite sizes and deformations of the crystal lattice in the crystallite (1), especially when discrepancy between the data in classic Williamson-Hall method indicates on the difference in sizes of crystallite and approximation assumed one mean size of crystallite cannot be efficiently applied. It base on the determination of the real widening of the selected diffraction line and in the case of the applied pseudo-Voigt function can be calculated from the formula:

$$\beta_C(f) = \beta_C(h) - \beta_C(i)$$

For the Cauchy component, and from the formula:

$$\beta_G(f) = \sqrt{\beta_G(h)^2 - \beta_G(i)^2}$$

for Gaussian component. Above $\beta_C(f), \beta_G(f)$, is the component of Cauchy and Gaussian, respectively, for the real (physical) widening of the diffraction line profile. The symbol $\beta_C(h)$ and $\beta_G(h)$ is the component of Cauchy and Gaussian, respectively, of the widening of the diffraction line profile designated in the experiment. The symbol $\beta_G(i)$ is the component of Cauchy and Gaussian, respectively, of an apparatus widening of the diffraction line profile. The Gaussian and Cauchy component of an apparatus widening of the diffraction line profile was determined from X-ray diffraction measurement of the standard sample, which was LaB_6 (NIST Standard Reference Powder 660a). All components of Cauchy and Gaussian of the widening of diffraction line were calculated using the empirical formulas described in [28]. Ultimately, the crystallite sizes was determined from the formula:

$$D_{Cr} = \frac{\lambda}{\beta_c(f)\cos\theta}$$

and deformation of the crystal lattice from the formula:

$$\varepsilon = \frac{\beta_G(f)}{4\mathrm{tg}\,\theta}$$

In this way, by choosing the reflexes 002 and 100, the characteristic microstructure parameters of the crystallite in two perpendicular directions were determined respectively i.e sizes (D_{Cr} = H and D_{Cr} = D) as also deformations of the crystal lattice ($\varepsilon = \varepsilon\_\parallel$ and $\varepsilon = \varepsilon\_\perp$).

The molecule size of organic additives (Table 1) were calculated using software SCIGRESS, Molecular modeling software, FQS Poland, ver. FJ-2.4.

3. Result and discussion

3.1. Selection of the optimum surfactants to assist in depositing Zn-Mo

3.1.1. Chemical analysis and SEM observations

Examination of chemical composition of the electrodeposited layers and calculation of the current efficiency of the electrodeposition process was the first part of investigations conducted to evaluate the impact of the addition of various organic compounds. The effect of polyethylene glycol various concentration was examined (Fig. 1). Result revealed that molybdenum content in the layer increases with increase of PEG concentration up to 0.50 g/dm^3 in electrolytic bath (Fig. 1a). Above the concentration of 0.50 g/dm^3 PEG in the bath, Mo amount in the electrodeposited layers remains in the constant level. The current efficiency values do not change in the whole range of PEG concentration studied. Nevertheless, it is also important to notice that the addition of only 0.05 g/dm^3 of dodecyl sulphate sodium salt (SDS) in the plating bath improve the current efficiency of the Zn-Mo layer electrodeposition process evidently (Fig. 1b).

Fig. 2a shows the surface of Zn-Mo layer obtained from a simple bath without any organic additives. It can be easily noticed that the coating obtained in such conditions is not compact and unevenly covers the surface. Fig. 2b demonstrate Zn-Mo coating obtained from the plating bath with SDS and without

PEG. The surface is built of various sized particles with sharp edges. Moreover the layer covers the substrate also uniformly. The current efficiency of Zn-Mo electrodeposition process increases from 65.96% to 73.20% for the bath without additives and with SDS respectively. Hence it can be stated that the addition of SDS to electrolytic bath is indispensable to obtain uniform films and improve the efficiency of the electrodeposition process.

Fig. 3 (a-h) presents SEM images of layers obtained from the bath with various concentration of PEG 3000 and PEG 20000. Except that the surface morphology varies depending on PEG molecular weight, it can be observed also that, in each investigated type of polyethylene glycol, the increase of PEG concentration in electrolyte solution result in the flattening of the surface of Zn-Mo layers obtained. Moreover, it can be suggested that the addition of PEG with lower molecular weight to the plating bath promotes the formation of needle shaped grains of Zn-Mo.

Next the effect of Triton X-100 addition was studied (Fig. 4). Small addition, of about 0.1 g/dm^3, of Triton X-100 (Fig. 4b), makes that Mo amount in the layer increase sharply in comparison to layer obtained in the presence of only SDS. Next, when higher amounts of Triton is added the Mo content decreases sharply. The addition of the lowest amount of Triton X-100 studied results in the formation of the needle-shape structure oriented parallel to the substrate (Fig. 4b). It is important to note that only small quantity allows to achieve good quality layer, but higher concentration of this nonionic surfactant results in the occurrence of a nodular developed structures (Fig. 4c-4f).

Subsequently, the influence of D-sorbitol was examined (Fig. 5). The addition of relatively high concentration of D-sorbitol cause considerable leveling of the deposits surface (Fig. 5f). Moreover, with increase of amount of D-sorbitol in the solution, the molybdenum content in the film increases significantly (Fig. 5a). Consequently, the increase of Mo content in the deposit enhances hydrogen co-evolution process, which results in the evident current efficiency decrease. Additionally, when the concentration of D-sorbitol is higher than 1.25 M
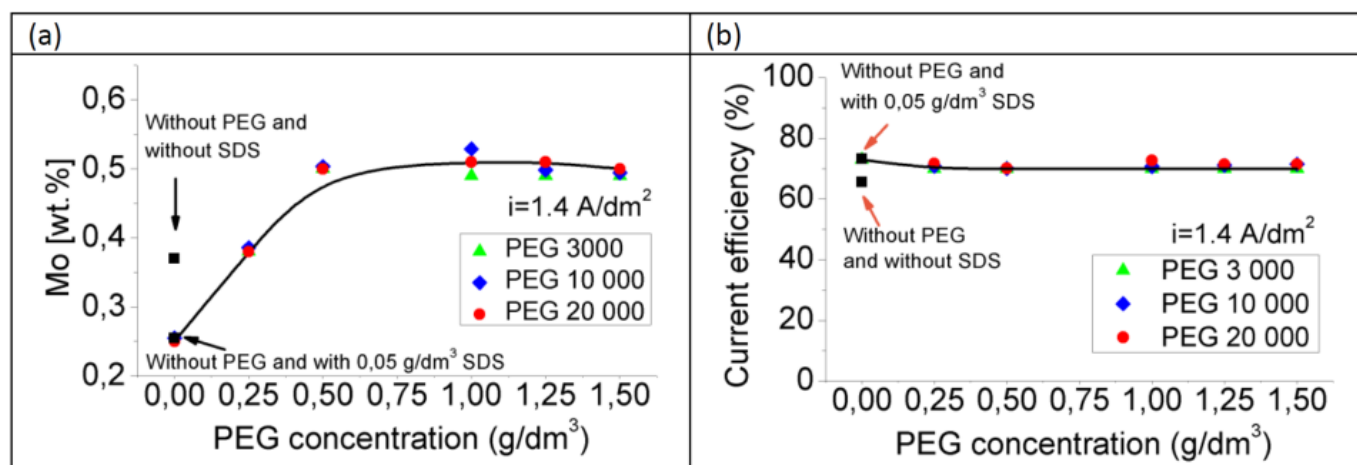

Fig. 1. Effect of polyethylene glycol concentration in electrolyte on the electrodeposition of Zn-Mo layers. (a) Mo content in deposits and (b) current efficiency of the electrodeposition process as a function of polyethylene glycol concentration in electrolyte. Electrodeposition conditions:, $i = -1.4$ A/dm^2, $Q = 30$ C, $\omega = 12.6$ rad/s, and T = 20°C, Fe substrate
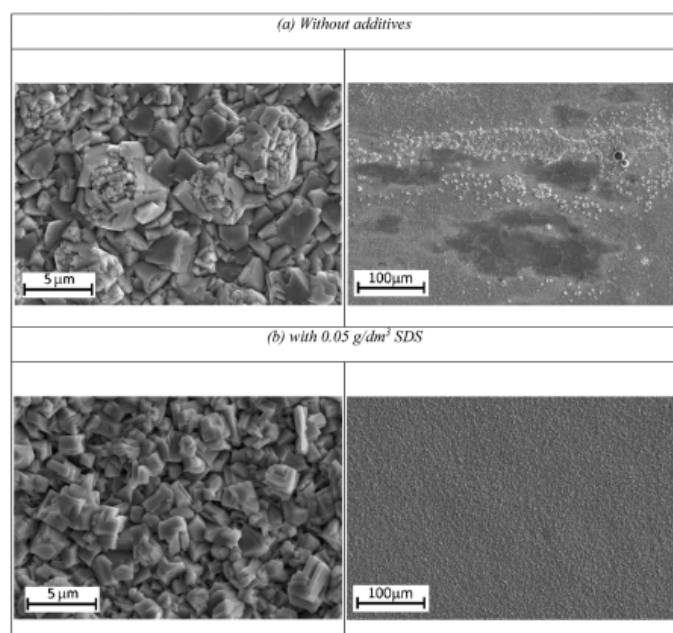
Fig. 2. SEM images (SE) of Zn-Mo coatings deposited from electrolytes without the presence of additives (a) and with the addition of SDS (b). Electrodeposition conditions: $i = -1.4$ A/dm^2, $Q = 30$ C, $\omega = 12.6$ rad/s, and $T = 20$°C, Fe substrate

such electrolyte solution become noticeably less efficient, and the drop of Mo content and current efficiency is observed. Furthermore, if the concentration of D-sorbitol in the solution reaches a value 1.5 M and more, molybdenum do not built into the layer. This phenomenon can be explained by exceeding the limit value of surfactant concentration in the solution, which prevents depositing a layer of Zn-Mo. After crossing the limit value, the surfactant adsorbs on the surface in a greater amount and consequently totally block the possibility of adsorption of Mo ions or complexes. The surface morphology changes from the sharp irregular to very compact and smooth with increasing content of D-sorbitol in the plating bath (Fig. 5 b-h). When the concentration of D-sorbitol is higher than 1.25 M the strong hydrogen evolution can conduct to increase of the near-surface pH and to presence of sorbitate anions (pH > 12) close to surface. Thus, it may be inferred that sorbitate anions favour deposition of finer Zn-Mo grains which is in line with the results noted by Pereira et al. [6] for zinc electrodeposition.

Successively, the effect of cationic surfactant CTAB was investigated (Fig. 6). It can be clearly visible that with increasing concentration of the additive in the bath, the Mo content in the layer growth sharply and reaches the value of approximately 1.0 wt. %. The presence of CTAB in concentration of 0.2 g/dm^3 and more maintains the Mo content at a constant level. As amount of CTAB rise in the solution, the current efficiency of the electrodeposition process decline up to about 40-60% (Fig. 6a).

The surface is smoother, with growing content of surfactant in the bath, and moreover the grains reaches porous needle like structure already using 0.2 g/dm^3 (similar effect of CTAB as determined by Gomes et al. [15] in case of zinc electrodeposition).
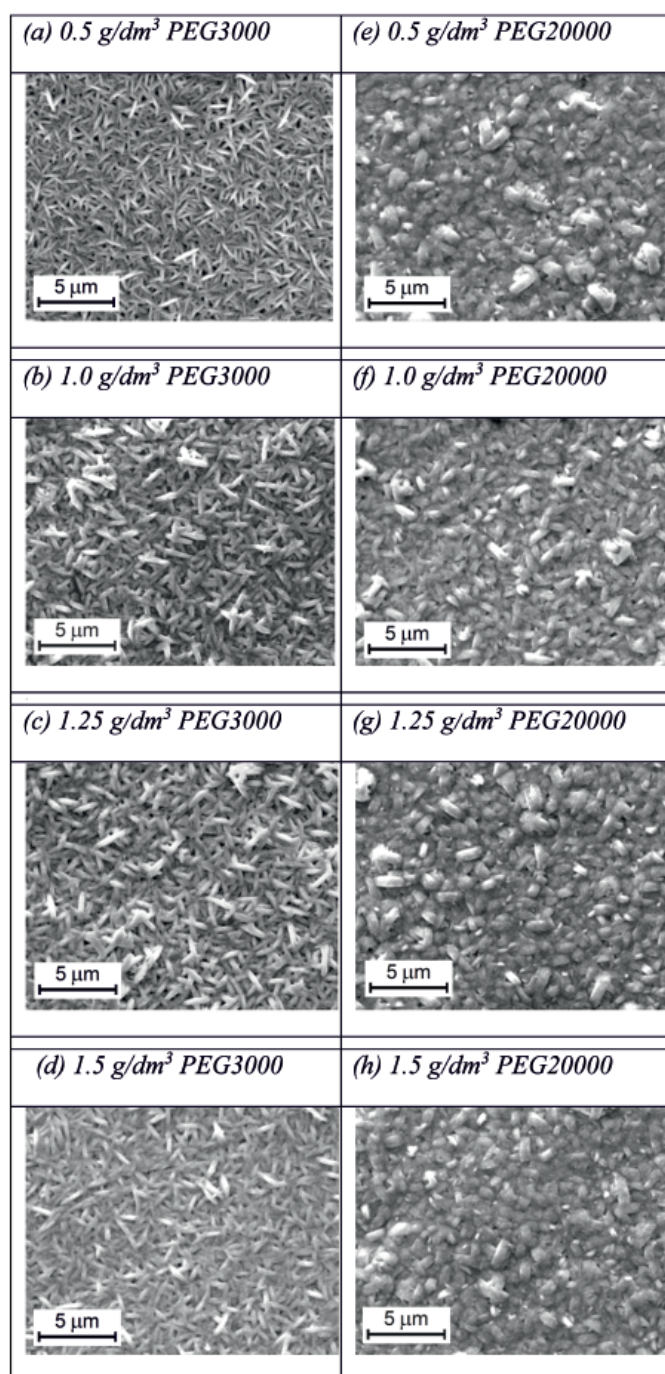

Fig. 3. SEM images (SE) of Zn–Mo coatings deposited from electrolytes with the addition of polyethylene glycol (PEG3000 and PEG20000) with various concentration (a-h). Electrodeposition conditions: $i = -1.4$ A/dm^2, $Q = 30$ C, $\omega = 12.6$ rad/s, and $T = 20$°C, Fe substrate

The effect of thiourea and of EDTA addition has been also tested, which both do not have any positive impact on the Zn-Mo electrodeposition process. In both cases considered the Mo content do not exceed 0.3 wt. % and deposited layers exhibit a highly developed surface (Fig. 7, Fig. 8).

The selection of the best working additives to second part of the research base on the comparison of a surface microstructure of the samples by SEM, molybdenum content in the deposits and current efficiency of the electrodeposition process (WDXRF).
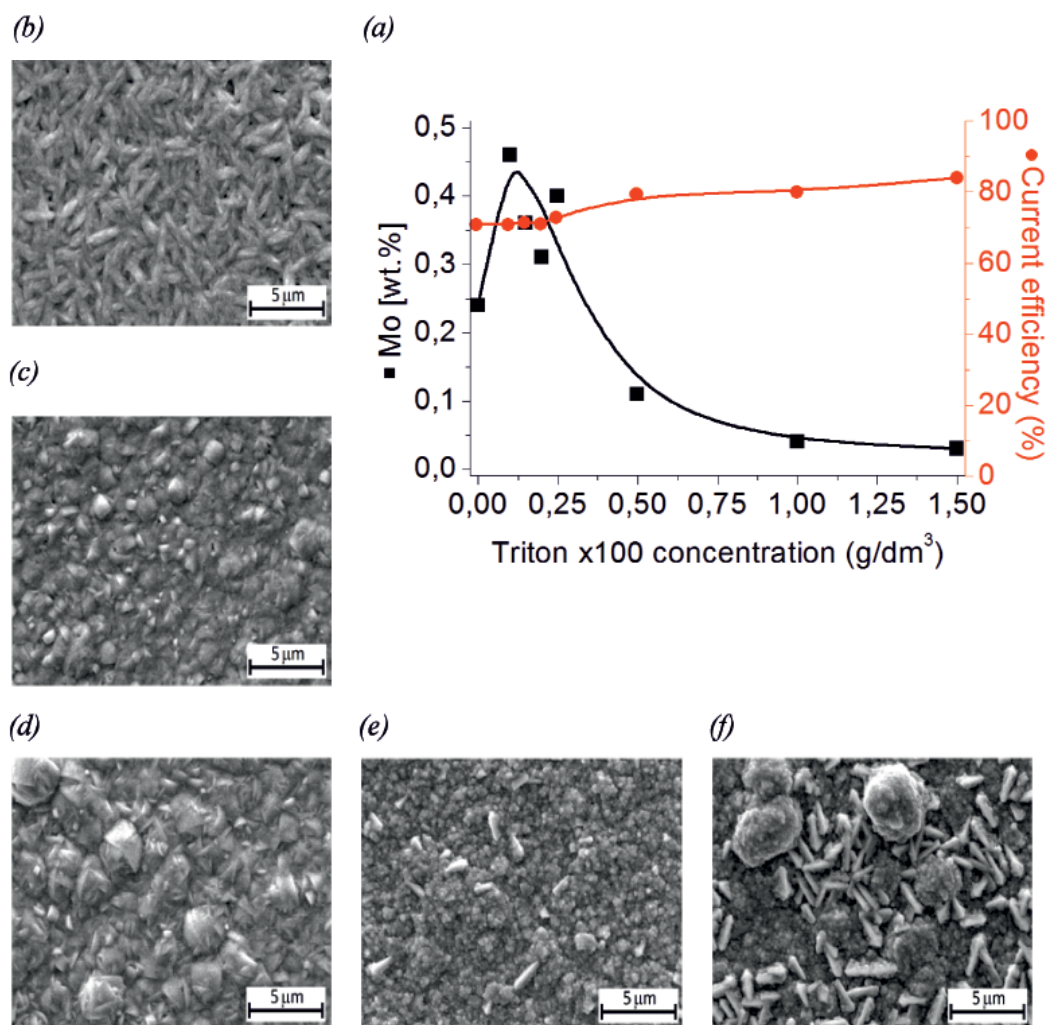
Fig. 4. Effect of Triton X-100 concentration in electrolyte on the electrodeposition of Zn-Mo layers. (a) Mo content in deposits and current efficiency of the electrodeposition process as a function of polyethylene glycol concentration in electrolyte. (b-f) SEM images (SE) of Zn–Mo coatings deposited from electrolytes with addition of Triton X-100 of various concentration. Electrodeposition conditions: $i = -1.4$ A/dm^2, $Q = 30$ C, $\omega = 12.6$ rad/s, and $T = 20°C$, Fe substrate

Figure 9 shows such comparison of electrodeposition process parameters. As it was mentioned above, the addition of SDS to the bath is prerequisite to ensure uniform surface coverage. It is clearly visible that the presence of PEG 20000, Triton X-100 and D-sorbitol proper amount makes that the electrodeposition process is the most efficient. Also, the coatings are smooth, compact and bright in the case of use such additives, so they will be the subject of further detailed investigation.

3.2. A detailed analysis of the impact of selected best-acting surfactants

3.2.1. AFM characterization

In order to examine the surface topography and roughness of zinc-molybdenum layers, the AFM analysis was carried out. All studied films were electrodeposited on steel substrate at the same current density ($i = -1.4$ A/dm^2) from electrolytes containing various additives. Achieved coatings were analyzed and compared by means of average roughness (R_a) (Fig. 11), kurtosis (S_{ku}) and skewness (S_{kk}) parameters (Fig. 12).

Figure 10 shows clearly the difference in the topography of the zinc-molybdenum coating with the addition of SDS and the rest of the studied samples. Comparing the grain size of a films electrodeposited with the presence of SDS in the bath and that with PEG 20000 or Triton X-100 or D-sorbitol or without surfactants, it can be seen that they were markedly larger. These results are in line with those illustrating the roughness (R_a) parameters (Fig. 11).

Although the structure of Zn-Mo layers with the addition of SDS seems to be relatively flat granular, the roughness measured was of 248 nm. Other considered additives such as PEG 20000, Triton X-100 and D-sorbitol shows a major decline of the surface roughness in comparison to layers obtained without the presence of surfactants in the plating baths. Moreover, the attendance of D-sorbitol in the solution cause clear reduction of grain size and the value of roughness parameter in relation to other studied surfactants (Fig. 10, 11). Furthermore, the values of skewness and kurtosis parameters of all considered samples
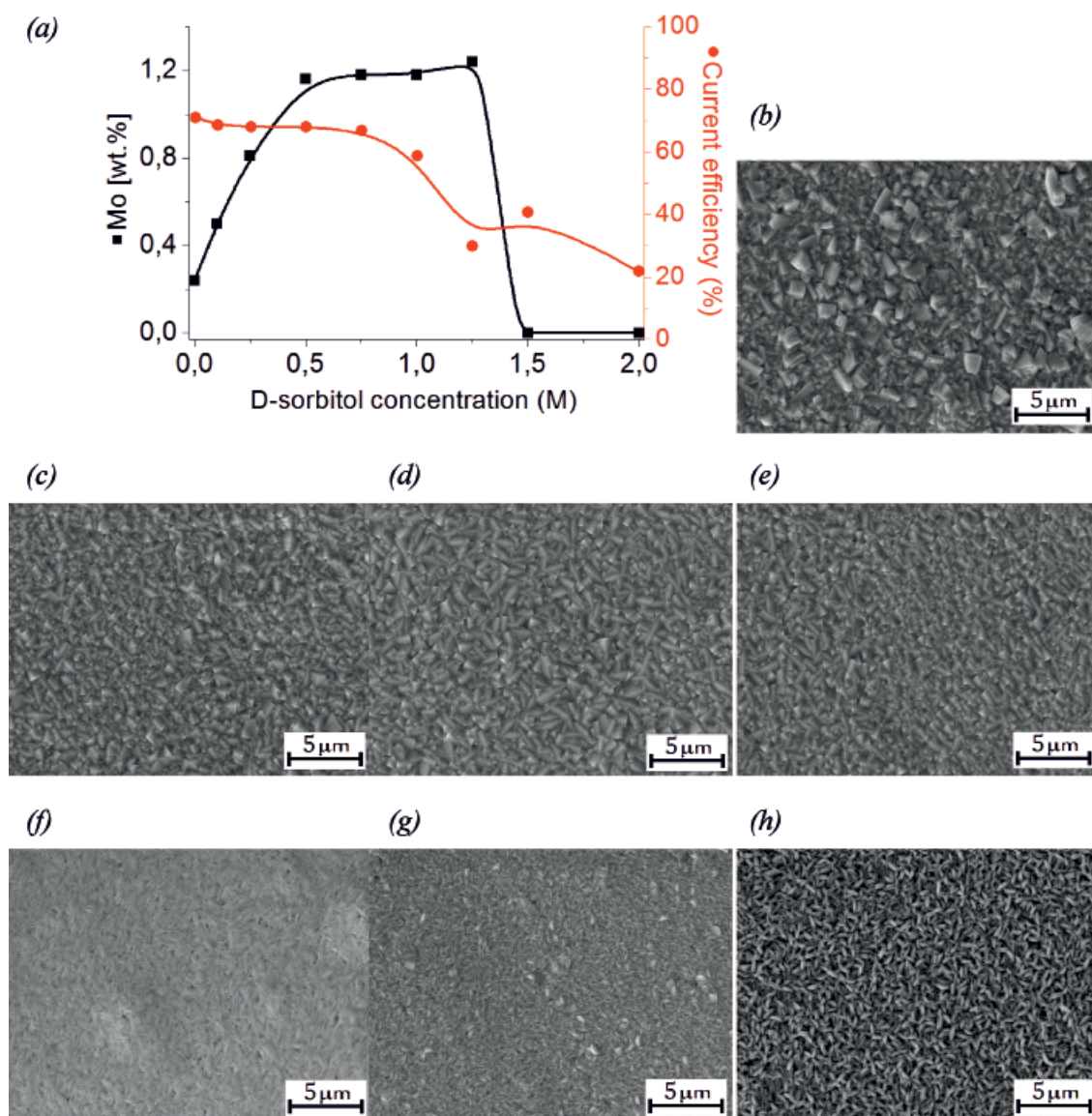
Fig. 5. Effect of D-sorbitol concentration in electrolyte on the electrodeposition of Zn-Mo layers. (a) Mo content in deposits and current efficiency of the electrodeposition process as a function of D-sorbitol concentration in electrolyte. (b-f) SEM images (SE) of Zn-Mo coatings deposited from electrolytes with addition of D-sorbitol of various concentration: 0,25 M (b), 0,5 M (c), 0,75 M (d), 1,0 M (e), 1,25 M (f), 1,5 M (g), 2,0 M (h). Electrodeposition conditions: $i = -1.4$ A/dm^2, $Q = 30$ C, $\omega = 12.6$ rad/s, and $T = 20°$C, Fe substrate

received with surface active additives are better or at least comparable to the values of such parameters in relation to steel substrate with certain little tendency of predominance of peaks. Hence, roughness profiles of their surfaces are close to ideal normal (Gaussian) distribution, which is given by roughness profile for skewness S_{kk} parameter equal 0.0 and for kurtosis S_{ku} parameter equal 3.0 (Fig. 12).

3.2.2. XRD Diffraction

X-ray structural studies of Zn-Mo films were carried out at room temperature directly after their deposition. The results have shown that obtaining alloy layers are characterized by the presence of one phase (baths with PEG 20000, Fig. 13a) or two phases (baths with Triton X-100 and D-sorbitol, Fig. 13 d, g).

The all above phases crystallize in the same hexagonal crystal system of the Zn type (hexagonal close-packed, A3 crystal structure). The first hexagonal phase is (Zn,Mo) phase with lower c/a ratio of cell parameters as a result of replacement of zinc atoms by molybdenum atoms in the Zn hexagonal crystal lattice (the higher atomic radius of molybdenum compared to the zinc atomic radius: 1.90 Å vs. 1.42 Å (35, 36)). The second hexagonal phase is the phase close to pure zinc hexagonal phase (phase present in baths with Triton X-100 and D-sorbitol) which indicates the possibility of two different reduction paths of Zn(II) and Mo(VI) depend on presence of surfactants on the surface. Microstructure parameters such as crystallite sizes ($D_{Cr} = H$ and $D_{Cr} = D$) and deformations of crystal lattice in crystallite ($\varepsilon = \varepsilon\_\parallel$ and $\varepsilon = \varepsilon\_\perp$) were determined from analysis of the diffraction peak as it was described in point 2. The crystallite sizes and the deformations of the crystal lattice in the crystallite of (Zn,Mo)
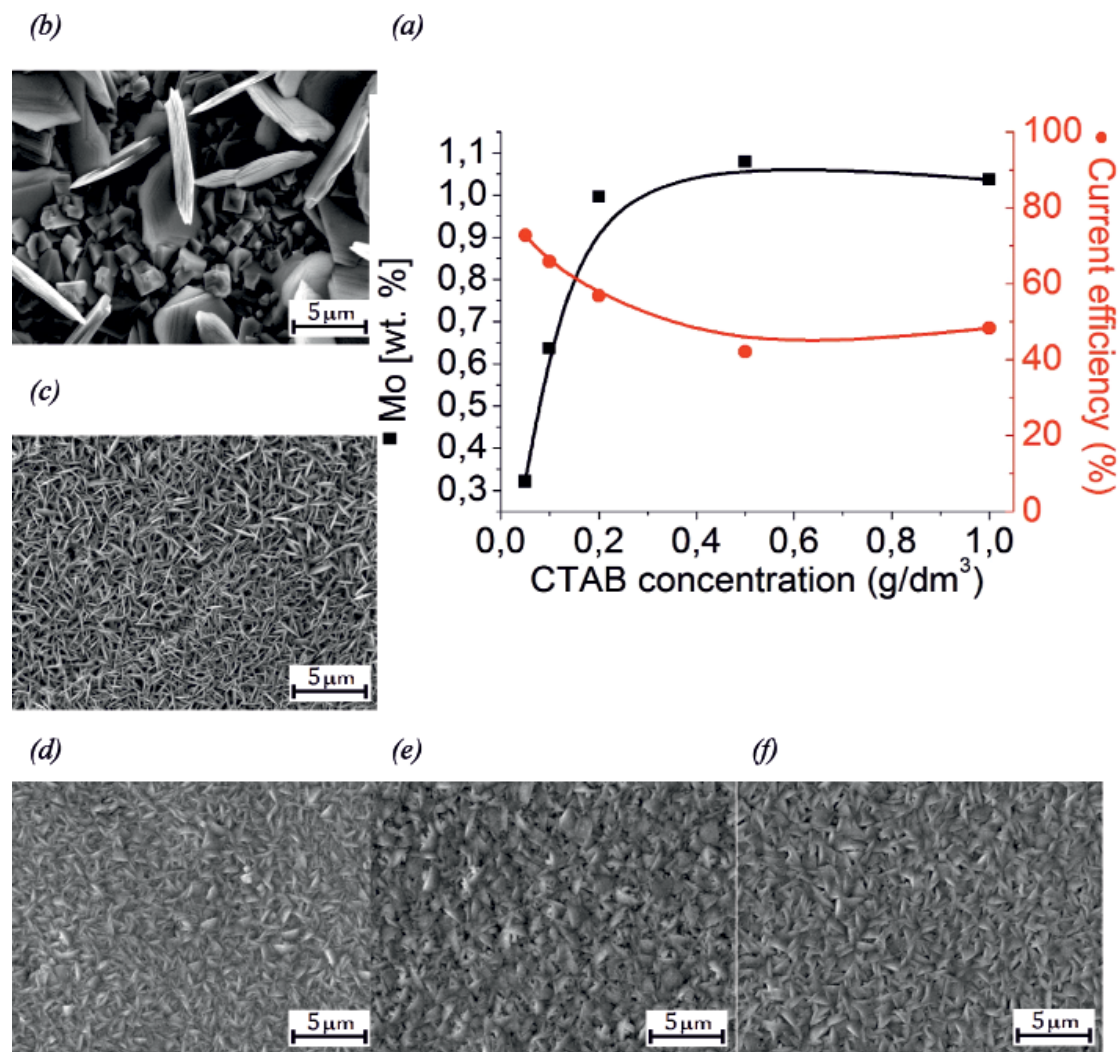
Fig. 6. Effect of CTAB addition in electrolyte on the electrodeposition of Zn-Mo layers. (a) Mo content in deposits and current efficiency of the electrodeposition process as a function of CTAB concentration in electrolyte. (b-f) SEM images (SE) of Zn–Mo coatings deposited from electrolytes with addition of CTAB of various concentration: 0,05 g/dm^3 (b), 0,1 g/dm^3 (c), 0,2 g/dm^3 (d), 0,5 g/dm^3 (e), 1,0 g/dm^3 (f). Electrodeposition conditions: $i = -1.4$ A/dm^2, $Q = 30$ C, $\omega = 12.6$ rad/s, and $T = 20°C$, Fe substrate

phase generally increases with growth of concentration of PEG 20000, but their changes not exceed 100 percent (Fig. 13b, 13c). The changes of crystallite sizes and deformations of the crystal lattice in the crystallite with growth of Triton X-100 concentration in baths are also very nearly in (Zn,Mo) phase, when in zinc phase (Zn) the crystallite sizes increase repeatedly and deformations of the crystal lattice in the crystallite decline significantly (Fig. 13e, 13f). The (Zn,Mo) and (Zn) phases are separate in case of D-sorbitol and below 1.2 M only (Zn,Mo) phase exist (Fig. 13h, 13i).

The increase of concentration of D-sorbitol in the electrolytic bath decline the crystallite sizes up to even 30 nm and 10 nm for D and H size parameters (the lowest crystallite sizes) at distortions of crystal lattice in the crystallite below $\varepsilon < 0.004$, when concentration of D-sorbitol reaches level 1.2 M. An abrupt change of chemical composition of layer for concertation of D-sorbitol about 1.3-1.5 M (Fig. 5) can indicate the instability of electrodeposition process, hence optimal concentration of D-sorbitol should be in stable region i.e. at about 0.75 M for

which the changes of concentration of surfactant don't change significantly chemical composition of layer.

3.2.3. Raman Spectroscopy

In order to verify the attendance of the oxides on the Zn-Mo layer the Raman Spectroscopy technique was applied. The Raman spectrum of the Zn-Mo layers in metal/metal oxides range (Raman shift from 50 to 1200 cm^{-1}) contains mainly peaks visible in Fig. 14 (inset graph). These peaks are related to hcp zinc and/or zinc-molybdenum phase (sharp peak about 71 cm^{-1}) as also to ZnO and (Zn,Mo)O oxides phases (broad band from about 400 to 620 cm^{-1} with maximum at 560-570 cm^{-1} [37]). The broad band for zinc oxide is characteristic to nonstoichiometric nanocrystalline oxide which contains vacancies of oxygen sites and this zinc oxide is different from bulk wurtzite ZnO phase [37]. Such nanocrystalline oxide can be difficult to determination by XRD technique. The influence of addition of
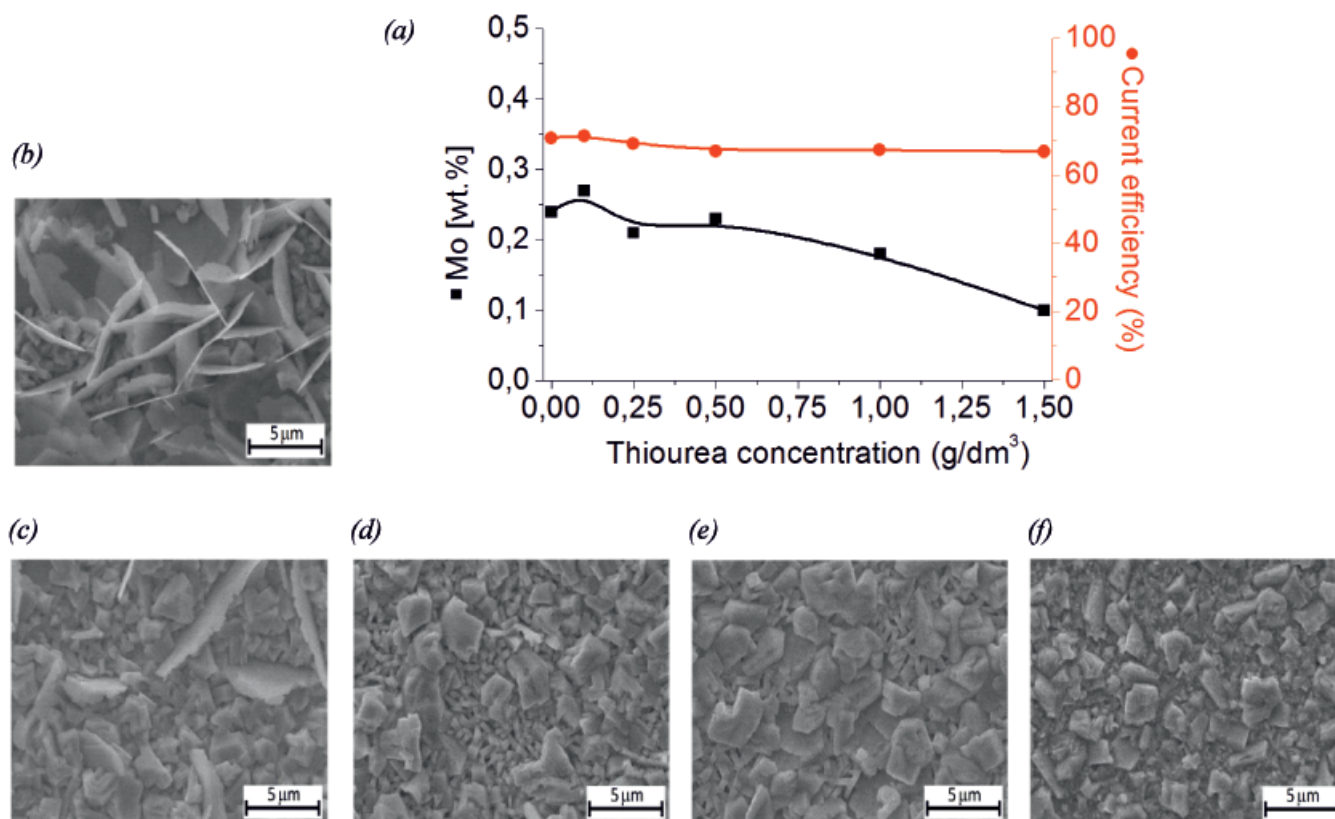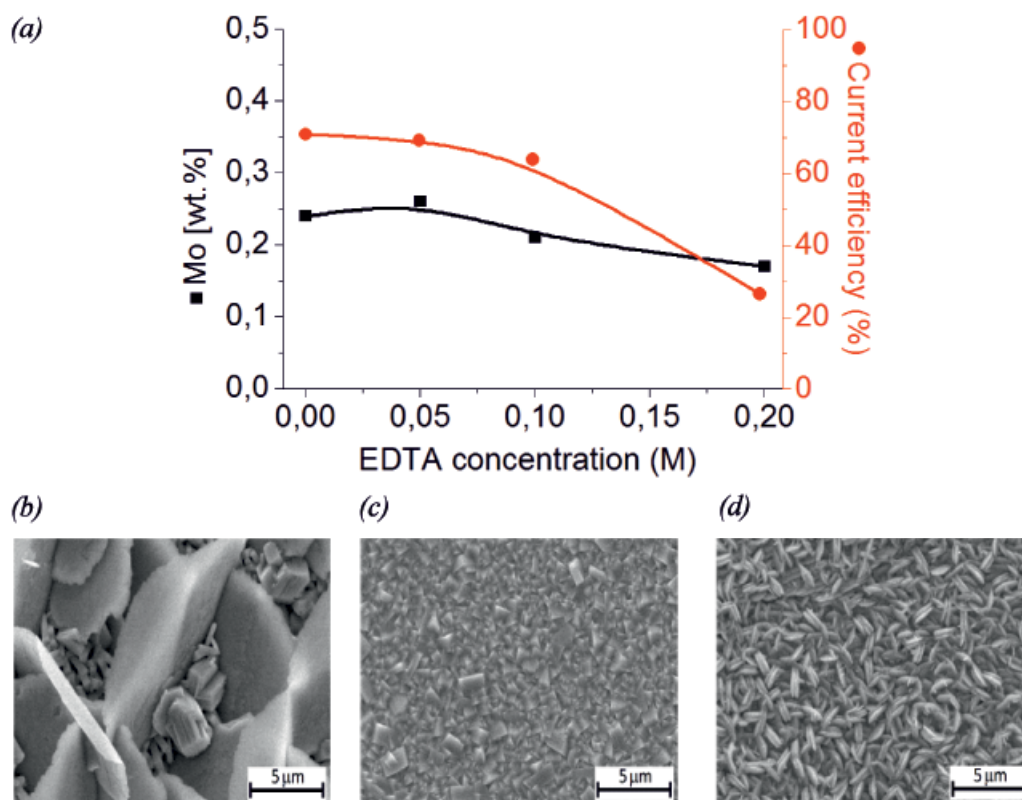
Fig. 7. Effect of Thiourea addition in electrolyte on the electrodeposition of Zn-Mo layers. (a) Mo content in deposits and current efficiency of the electrodeposition process as a function of Thiourea concentration in electrolyte. (b-f) SEM images (SE) of Zn-Mo coatings deposited from electrolytes with addition of Thiourea of various concentration. Electrodeposition conditions: $i = -1.4$ A/dm^2, $Q = 30$ C, $\omega = 12.6$ rad/s, and $T = 20°C$, Fe substrate

Fig. 8. Effect of EDTA addition in electrolyte on the electrodeposition of Zn-Mo layers. (a) Mo content in deposits and current efficiency of the electrodeposition process as a function of EDTA concentration in electrolyte. (b-d) SEM images (SE) of Zn-Mo coatings deposited from electrolytes with addition of EDTA of various concentration. Electrodeposition conditions: $i = -1.4$ A/dm^2, $Q = 30$ C, $\omega = 12.6$ rad/s, and $T = 20°C$, Fe substrate
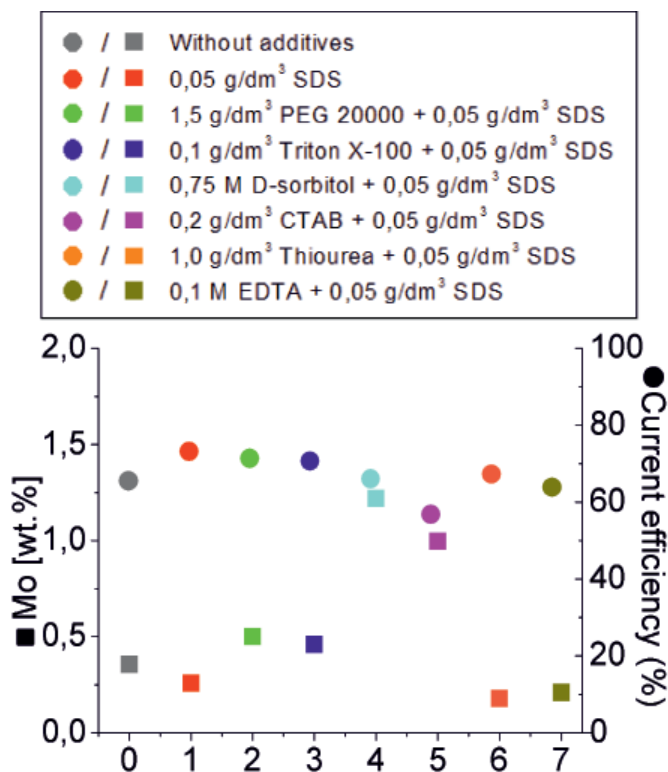
Fig. 9. Comparison of Mo content in deposits and current efficiency of the electrodeposition process for various additives studied. Electrodeposition conditions: $i = -1.4$ A/dm^2, $Q = 30$ C, $\omega = 12.6$ rad/s, and $T = 20$°C, Fe substrate

PEG, Triton X-100 and D-sorbitol on the oxidation of grains of electrodeposited layers is visible on figure 14. It is clearly observable that the level of oxidation of the surface differs for various organic compounds studied.

The disappearance of the zinc-molybdenum oxide Raman band at 560 cm^{-1} suggests that the presence of surface active additives in electrolytic bath cause essential decrease of oxides content in layers of Zn-Mo. The intensity of oxide Raman band decrease about 50%, 65% and 90% in presence of optimal concentration of D-sorbitol, Triton X-100 and PEG 20000 respectively. The results of Raman Spectroscopy for the layer electrodeposited with the presence in the solution of polyethylene glycol (PEG) indicate that the grains of the film are oxidized in the lowest extent. Thus it can by concluded that PEG with molecular weight 20 000 makes that the surface of Zn-Mo layers are weakly or not at all oxidized.
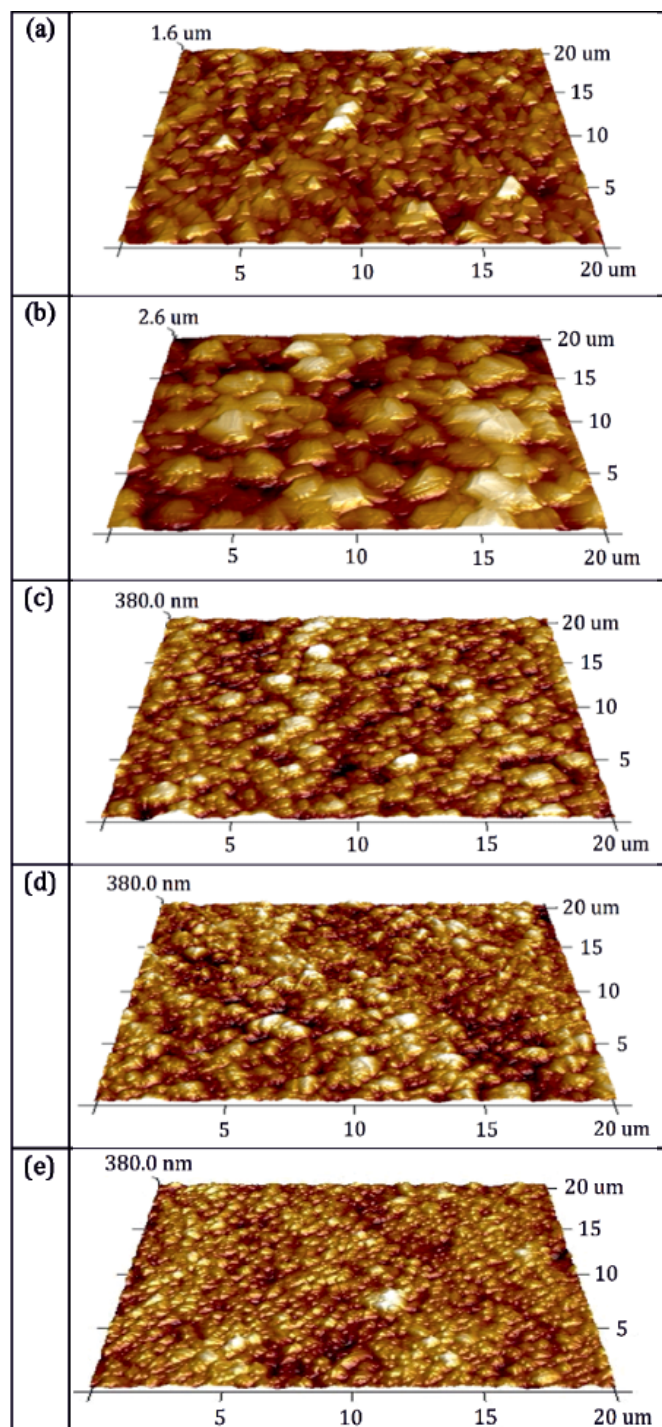

Fig. 10. AFM images of Zn-Mo layers without the addition of surfactants (a), with SDS (b), PEG 20000 (c), Triton X-100 (d) and D-sorbitol (e). Electrodeposition conditions: $i = -1.4$ A/dm^2, $Q = 30$ C, $\omega = 12.6$ rad/s and $T = 20$°C, Fe substrate

4. Conclusions

The Zn-Mo alloy coatings may be achieved by electrodeposition from stable citrate solutions with the addition of appropriate concentration of selected additives, with the current efficiency of the process about 70 %. The addition of proper amounts of PEG 20 000, D-sorbitol and Triton X-100 to the electrolytic bath results in the formation of uniform, smooth and bright Zn-Mo coatings. The results revealed the smallest roughness of Zn-Mo

alloy obtained from baths with PEG 20 000 (1.5 g/dm^3), D-sorbitol (0.75 M) and Triton X-100 (0.1 g/dm^3). XRD analysis confirm the presence of only one major hexagonal (Zn,Mo) phase in layers obtained from baths with addition of PEG 20000 as also presence of two hexagonal phases (hcp: (Zn,Mo) and Zn) in presence of D-sorbitol and Triton X-100. Proper amount of organic additives causes the decrease of crystallite sizes and the decrease of lattice deformations. The Zn-Mo layers with the low-
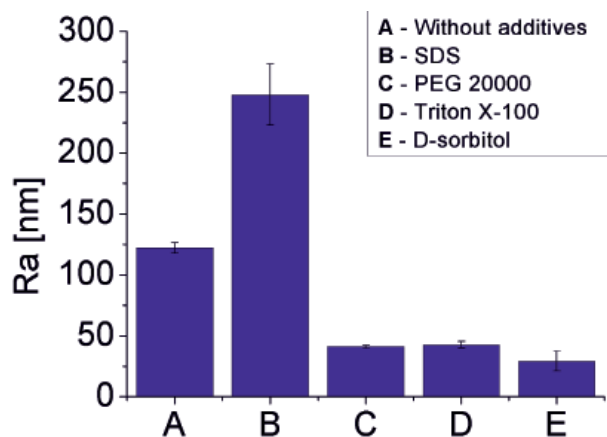
Fig. 11. The values of the average roughness (R_a) of the Zn-Mo coatings electrodeposited from the bath containing various surfactants and without it; Electrodeposition conditions: $i = -1.4$ A/dm^2, $Q = 30$ C, $\omega = 12.6$ rad/s and $T = 20°C$, Fe substrate

est oxidation of grains was gained from electrolytic bath with the addition of PEG 20 000. The presence of surface active additives in electrolytic bath cause essential decrease of oxides content in layers of Zn-Mo. The intensity of oxide Raman band decrease about 50%, 65% and 90% in presence of optimal concentration of D-sorbitol, Triton X-100 and PEG 20000 respectively.

REFERENCES

[1] N. Eliaz, E. Gileadi, Modern Aspects of Electrochemistry. **42**, Springer, New York (2008).
[2] H. Kazimierczak, P. Ozga, R.P. Socha, Electrochim. Acta. **104**, 378 – 390 (2013).
[3] R. Winand, J. Appl. Electrochem. **21**, 377-385 (1991).
[4] L.E. Morón, A. Méndez, F. Castañeda, J.G. Flores, L. Ortiz-Frade, Y. Meas, G. Trejo, Surf. Coat. Tech. **205**, 4985-4992 (2011).
[5] J.C. Ballesteros, P. D´ıaz-Arista, Y. Meas, R. Ortega, G. Trejo, Electrochim. Acta. **52**, 3686-3696 (2007).
[6] M.S. Pereira, L.L. Barbosa, C.A.C. Souza, A.C.M. De Moraes, I.A. Carlos, J. Appl. Electrochem. **36**, 727-732 (2006).
[7] H. Kazimierczak, Electrodeposition of Zn-Mo Layers from aqueous citrate solution, Polska Akademia Nauk, Kraków (2014).
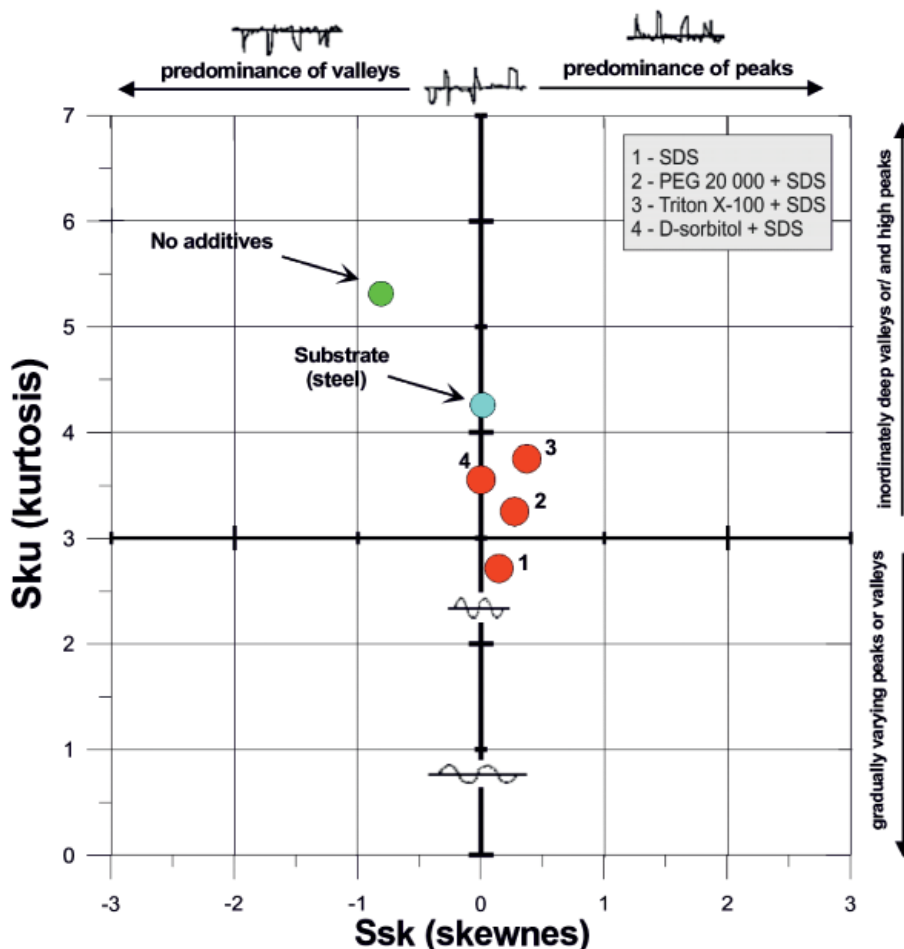

Fig. 12. Surface roughness characteristics, based on S_{ku} and S_{kk} parameters, for steel substrate, Zn-Mo without additives and with various surface active additives. Electrodeposition conditions: $i = -1.4$ A/dm^2, $Q = 30$ C, $\omega = 12.6$ rad/s and $T = 20°C$, Fe substrate
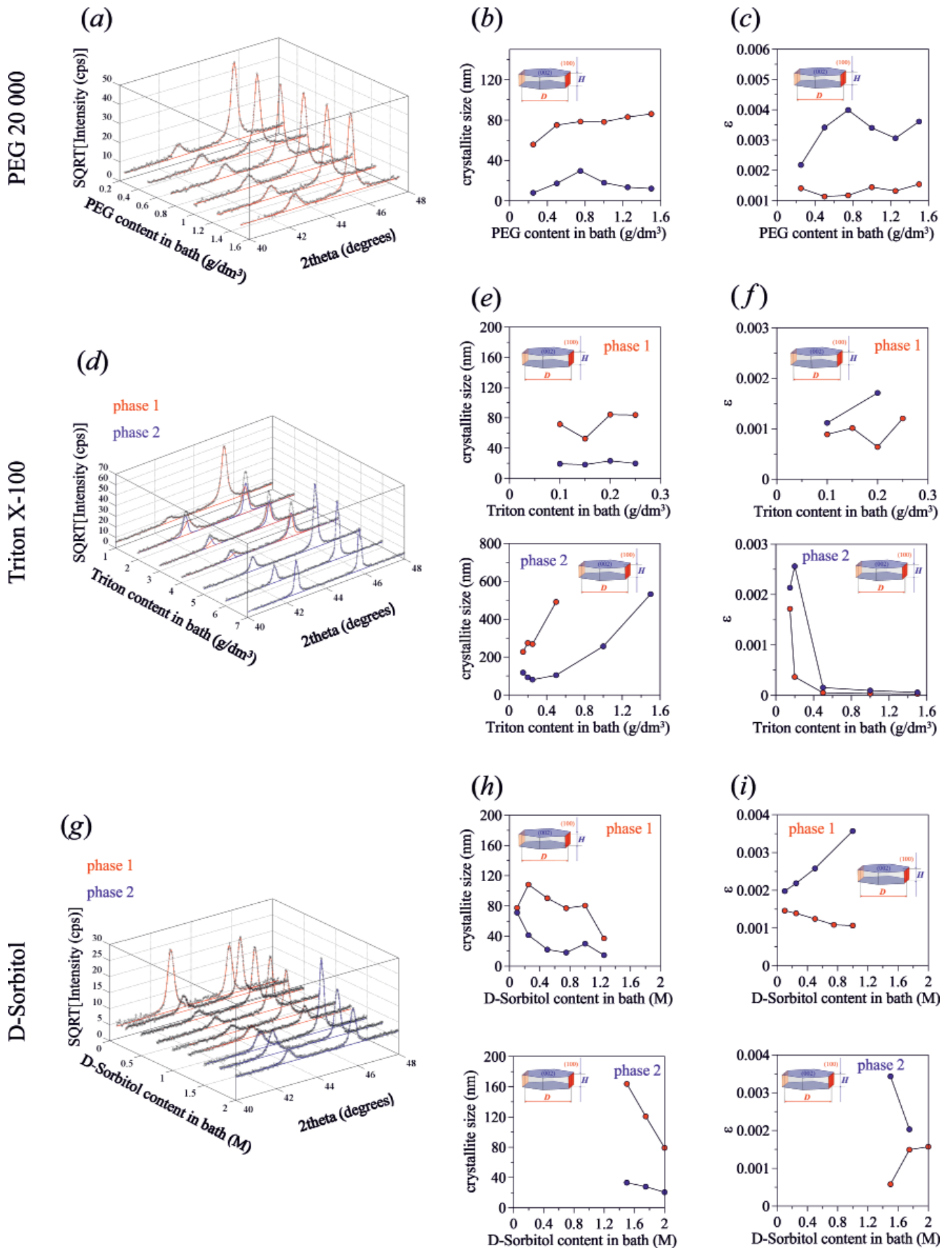
Fig. 13. X-Ray Diffraction patterns of the Zn-Mo coatings (a, d, g), the values of crystallite size (b, e, h) and the crystal lattice deformation (c, f, i). Electrodeposition conditions: $i = -1.4$ A/dm^2, $Q = 30$ C, $\omega = 12.6$ rad/s and $T = 20°C$, Fe substrate.
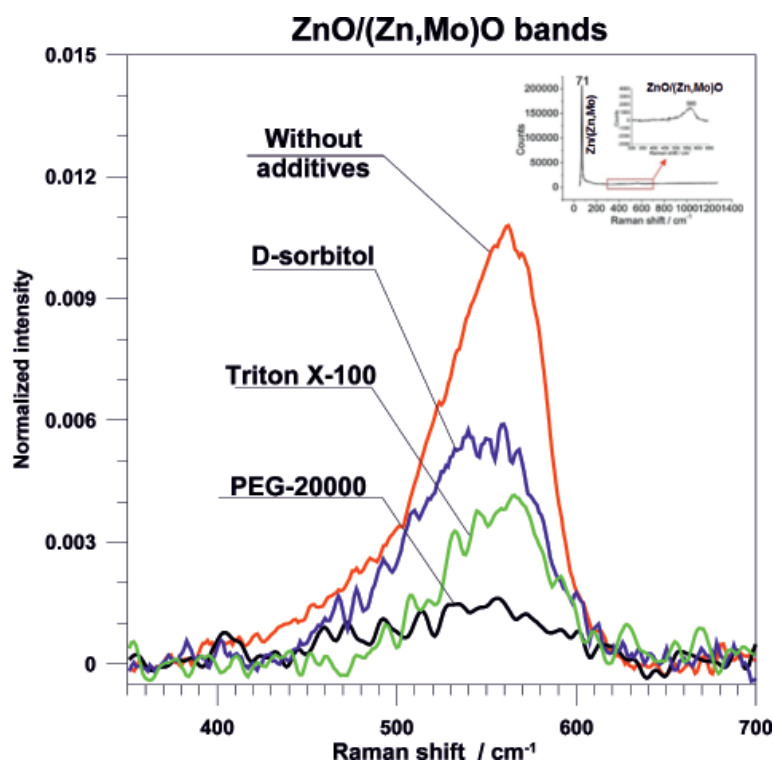
Fig. 14. Raman spectra of zinc-molybdenum oxide bands of layers electrodeposited from baths containing additions of Triton X-100, PEG 20000, D-sorbitol as also from bath without addition of surfactants. The inset graph presents typical Raman spectrum of coating in the range 50-1200 cm^{-1} which contains sharp peak from hcp zinc and zinc-molybdenum phases (about 71 cm^{-1}) as also broad band from oxide phases with maximum at 560 cm^{-1} (the fragment of spectrum for oxide phase is shown). The intensities are normalized by the maximum value of peak from hcp phase(s)

[8] G. Trejo, H. Ruiz, R. Ortega Borges, Y. Meas, J. Appl. Electrochem. **31**, 689-692 (2001).

[9] A. Sharma, K. Das, H.J. Fecht, S. Das, Appl. Surf. Sci. **314**, 516-522 (2014).

[10] C.M. Praveen Kumar, T.V. Venkatesha, K.G. Chandrappa, Surf. Coat. Tech. **206**, 2249-2257 (2012).

[11] H. Usui, Electrochim. Acta. **56**, 3934-3940 (2011).

[12] M.F. Carvalho, E.P. Barbano, I.A. Carlos, Electrochim. Acta. **109**, 798-808 (2013).

[13] I.L. Lehr, S.B. Saidman, Appl. Surf. Sci. **258**, 4417-4423 (2012).

[14] X. Zhang, J. Liang, B. Liu, Z. Peng, Colloid. Surface. A. **454**, 113-118 (2014).

[15] A.Gomes, M.I. da Silva Pereira, Electrochim. Acta. **51**, 1342-1350 (2006).

[16] X. Qin, G. Shao, L. Zhao, Mater. Sci. Eng. B-Adv. **177**, 1678-1681 (2012).

[17] M.F. Carvalho, I.A. Carlos, Electrochim. Acta. **113**, 229-239 (2013).

[18] H. Nakano, S. Oue, Y. Hamaguchi, S. Kobayashi, H. Fukushima, Tetsu-to-Hagane. **96** (6), (2010).

[19] J.L. Ortiz-Aparicio, Y. Meas, G. Trejo, R.I. Ortega, T.W. Chapman, E. Chainet, J. Appl. Electrochem. **43**, 289-300 (2013).

[20] S. Shanmugasigamani, M. Pushpavanam, Electrochim. Acta. **27**, 725-735 (2009).

[21] F. Galvani, I.A. Carlos, Met. Finish, 70-71 (1997).

[22] X. Wu, Z. Liu, X. Liu, Hydrometallurgy **141**, 31-35 (2014).

[23] M. Chandran, R.L. Sarma, R.M Krishnan, B. Electrochem. **15** (7-8), 242-247 (1999).

[24] https://media.beckman.com/-/media/pdf-assets/application--notes/particle-delsamax-application-note-hydrodynamic-size-surfactant-micelles.pdf., Beckman Coulter, Inc. USA (2013).

[25] W. Guo, Y.W. Sun, G.S. Luo, Y.J. Wang, Colloid. Surface. A. **252**, 71-77 (2005).

[26] S.K. Mehta, S. Kumar, M. Gradzielski, J. Colloid Interf. Sci. **360**, 497-507 (2011).

[27] H.S. Maharana, A. Basu, Surf. Coat. Tech. **310**, 148-156 (2017).

[28] T.H. de Keijser, J.I. Langrord, E.J. Mittemeijer, A.B.P. Vogels, J. Appl. Crystallogr. **15**, 308-314 (1982).

[29] H. Kazimierczak, P. Ozga, A. Jałowiec, R. Kowalik, J. Alloy. Compd. **578**, 82-89 (2013).

[30] P. Blake, P.D. Brimicombe, R.R. Nair, T.J. Booth, D. Jiang, F. Schedin, L.A. Ponomarenko, S.V. Morozov, H.F. Gleeson, E.W. Hill, A.K. Geim, K.S. Novoselov, Nano Lett. **8** (6), 1704-1708 (2008).

[31] A. Mendez, Y. Meas, R. Ortega-Borges, G. Trejo, J. Electrochem. Soc. **159** (3), 48-55 (2012).

[32] M. Nunez, Metal Electrodeposition, Nova Science Publishers Inc., New York (2005). ISBN: 1-59454-456-5.

[33] H. Lee, R.M. Vanable, A.D. MacKerell Jr., R.W. Pastor, Biophys. J. **95**, 1590-1599 (2008).

[34] H.H. Paradies, J. Phys. Chem.-US. **84** (6), 599-607 (1980).

[35] E. Clementi, D.L. Raimondi, J. Chem. Phys. **38**, 2686-2689 (1963).

[36] E. Clementi, D.L. Raimondi, W.P. Reinhardt, J. Chem. Phys. **47**, 1300–1307 (1967).

[37] C. Cachet, F. Ganne, S. Joiret, G. Maurin, J. Petitjean, V. Vivier, R. Wiart, Electrochim. Acta. **47**, 3409-3422 (2002).